Supporting Information

Assembly of BF_4^-, PF_6^-, ClO_4^- and F^- with trinuclear copper(I) acetylide complexes bearing amide groups: Structural diversity, photophysics and anion binding properties

Hua-Yun Shi, Yong-Liang Huang, Jia-Kai Sun, Ji-Jun Jiang, Zhi-Xing Luo, Hui-Tao Ling, Chi-Keung Lam and Hsiu-Yi Chao[*]

MOE Key Laboratory of Bioinorganic and Synthetic Chemistry, School of Chemistry and Chemical Engineering, Sun Yat-Sen University, Guangzhou 510275, P. R. China

Table S1. Crystallographic data for **1·BF₄**, **1·PF₆** and **1·ClO₄**.

	1·BF₄	1·PF₆	1·ClO₄
Formula	$C_{105}H_{83.5}BCu_3F_4N_4O_6P_6$	$C_{216}H_{177}Cu_6F_{12}N_{11}O_{12}P_{14}$	$C_{105}H_{84}ClCu_3N_4O_{10}P_6$
M (g/mol)	1960.51	4161.51	1973.65
cryst syst	Orthorhombic	Orthorhombic	Orthorhombic
space group	Pccn	Pccn	Pccn
a (Å)	22.4406(2)	37.4996(2)	37.5964(4)
b (Å)	37.5572(3)	22.30710(10)	22.4534
c (Å)	23.51116(19)	23.64730(10)	23.4691(2)
α (°)	90	90	90
β (°)	90	90	90
γ (°)	90	90	90
V (Å³)	19815.3(3)	19781.14(16)	19811.8(4)
Z	8	4	8
D_c (g cm⁻³)	1.314	1.397	1.323
T (K)	293(2)	150(2)	150(2)
reflns collected	76185	93931	46763
indep reflns	16018	17425	17318
R_{int}	0.0365	0.0347	0.0364
R^a, R_w^b [$I > 2\sigma(I)$]	0.0733, 0.1948	0.0699, 0.2008	0.0604, 0.1454
GOF on F²	1.091	1.088	1.060

[a] $R = \Sigma(|F_0|-|F_c|)/\Sigma|F_0|$ [b] $R_w = [\Sigma w(|F_0|-|F_c|)^2/\Sigma w(|F_0|)^2]^{1/2}$

Table S2. Crystallographic data for **2·BF₄** and **3·BF₄**.

	2·BF₄	**3·BF₄**
Formula	$C_{107}H_{84}BCu_3F_{10}N_2O_2P_6$	$C_{420}H_{343}B_4Cu_{12}F_{16}N_8O_8P_{24}$
M (g/mol)	2007.01	7483.02
cryst syst	monoclinic	monoclinic
space group	C2/c	Pc
a (Å)	29.9632(4)	27.5828(2)
b (Å)	22.3042(3)	28.8914(2)
c (Å)	30.6835(4)	24.54769(19)
α (°)	90.00	90.00
β (°)	101.1740(10)	103.7049(8)
γ (°)	90.00	90.00
V (Å³)	20117.2(5)	19005.2(3)
Z	8	2
D_c (mg cm⁻³)	1.325	1.308
T (K)	293(2)	293(2)
reflns collected	55840	87165
indep reflns	17654	41477
R_{int}	0.0392	0.0325
R^a, R_w^b [$I > 2\sigma(I)$]	0.0412, 0.1085	0.0392, 0.1005
GOF on F^2	1.056	1.016

[a] $R = \Sigma(|F_0|-|F_c|)/\Sigma|F_0|$ [b] $R_w = [\Sigma w(|F_0|-|F_c|)^2/\Sigma w(|F_0|)^2]^{1/2}$

Table S3. Crystallographic data for **4·BF₄** and **4·F**.

	4·BF₄	**4·F**
Formula	$C_{107}H_{90}BCu_3F_4N_2O_4P_6$	$C_{107}H_{90}Cu_3FN_2O_4P_6$
M (g/mol)	1931.06	1863.25
cryst syst	monoclinic	monoclinic
space group	$P2_{1/c}$	$P2_1/n$
a (Å)	22.36838(19)	17.90690(10)
b (Å)	34.9812(3)	23.0779(2)
c (Å)	25.4082(2)	27.5279(3)
α (°)	90.00	90.00
β (°)	90.3117(8)	104.6560(10)
γ (°)	90.00	90.00
V (Å³)	19881.0(3)	11005.85(17)
Z	8	4
D_c (mg cm⁻³)	1.290	1.124
T (K)	150(2)	173(2)
reflns collected	130764	48380
indep reflns	34881	19328
R_{int}	0.0488	0.0378
R^a, $R_w{}^b$ [$I > 2\sigma(I)$]	0.1195, 0.3058	0.0444, 0.1233
GOF on F^2	1.066	1.029

[a] $R = \Sigma(|F_0|-|F_c|)/\Sigma|F_0|$ [b] $R_w = [\Sigma w(|F_0|-|F_c|)^2/\Sigma w(|F_0|)^2]^{1/2}$

Table S4. Selected bond lengths (Å) and angles (°) for **1·BF₄** and **1·ClO₄**.

1·BF₄		1·ClO₄	
Cu(1)···Cu(2)	2.7378(10)	Cu(1)···Cu(2)	2.5709(8)
Cu(1)···Cu(3)	2.5438(9)	Cu(1)···Cu(3)	2.7466(8)
Cu(2)···Cu(3)	2.5644(10)	Cu(2)···Cu(3)	2.5473(7)
C(83)–Cu(1)	2.409(5)	C(1)–Cu(1)	2.318(4)
C(83)–Cu(2)	2.176(5)	C(1)–Cu(2)	2.111(4)
C(83)–Cu(3)	2.071(5)	C(1)–Cu(3)	2.130(4)
C(99)–Cu(1)	2.128(5)	C(16)–Cu(1)	2.168(4)
C(99)–Cu(2)	2.302(5)	C(16)–Cu(2)	2.076(4)
C(99)–Cu(3)	2.107(5)	C(16)–Cu(3)	2.423(4)
Cu(1)–P(4)	2.2605(14)	Cu(1)–P(1)	2.2945(11)
Cu(1)–P(5)	2.2946(14)	Cu(1)–P(6)	2.2662(12)
Cu(2)–P(6)	2.2677(16)	Cu(2)–P(2)	2.2845(10)
Cu(2)–P(7)	2.2978(14)	Cu(2)–P(3)	2.2838(11)
Cu(3) –P(8)	2.2822(13)	Cu(3) –P(4)	2.2949(11)
Cu(3)–P(9)	2.2835(14)	Cu(3)–P(5)	2.2598(11)
C(83)–C(84)	1.207(7)	C(1)–C(2)	1.203(5)
C(99)–C(100)	1.219(7)	C(16)–C(17)	1.207(6)
C(91)–O(114)	1.223(7)	C(9)–O(1)	1.216(5)
C(107)–O(117)	1.218(6)	C(24)–O(4)	1.224(6)
N(121)–O(118)	1.232(8)	N(2)–O(2)	1.223(6)
N(121)–O(119)	1.224(9)	N(2)–O(3)	1.226(6)
N(123)–O(115)	1.235(7)	N(4)–O(5)	1.223(6)
N(123)–O(116)	1.224(7)	N(4)–O(6)	1.216(6)
C(84)–C(83)–Cu(1)	122.6(4)	C(2)–C(1)–Cu(1)	124.6(3)
C(84)–C(83)–Cu(2)	126.3(4)	C(2)–C(1)–Cu(2)	149.3(3)
C(84)–C(83)–Cu(3)	157.4(5)	C(2)–C(1)–Cu(3)	132.7(3)
C(100)–C(99)–Cu(1)	132.5(4)	C(17)–C(16)–Cu(1)	125.8(3)
C(100)–C(99)–Cu(2)	124.8(4)	C(17)–C(16)–Cu(2)	157.3(4)
C(100)–C(99)–Cu(3)	149.1(4)	C(17)–C(16)–Cu(3)	123.6(3)
Cu(1)–C(83)–Cu(2)	73.14(15)	Cu(1)–C(1)–Cu(2)	70.78(11)
Cu(1)–C(83)–Cu(3)	68.72(15)	Cu(1)–C(1)–Cu(3)	76.12(12)
Cu(2)–C(83)–Cu(3)	74.25(16)	Cu(2)–C(1)–Cu(3)	73.81(12)
Cu(1)–C(99)–Cu(2)	76.22(15)	Cu(1)–C(16)–Cu(2)	74.54(13)
Cu(1)–C(99)–Cu(3)	73.83(15)	Cu(1)–C(16)–Cu(3)	68.48(12)
Cu(2)–C(99)–Cu(3)	70.98(14)	Cu(2)–C(16)–Cu(3)	68.48(12)

Table S5. Selected bond lengths (Å) and angles (°) for **2·BF₄** and **3·BF₄**

2·BF₄		3·BF₄	
Cu(1)···Cu(2)	2.8375(5)	Cu(1)···Cu(2)	2.5908(8)
Cu(1)···Cu(3)	2.6987(5)	Cu(1)···Cu(3)	2.5774(8)
Cu(2)···Cu(3)	2.4944(4)	Cu(2)···Cu(3)	2.6297(8)
C(117)–Cu(1)	2.018(2)	C(1)–Cu(1)	2.251(4)
C(117)–Cu(2)	2.317(2)	C(1)–Cu(2)	2.080(4)
C(117)–Cu(3)	2.157(2)	C(1)–Cu(3)	2.223(4)
C(119)–Cu(2)	2.079(2)	C(16)–Cu(1)	2.121(4)
C(119)–Cu(3)	2.041(2)	C(16)–Cu(2)	2.222(4)
Cu(1)–P(1)	2.2991(6)	C(16)–Cu(3)	2.174(4)
Cu(1)–P(6)	2.2901(6)	Cu(1)–P(1)	2.2716(12)
Cu(2)–P(4)	2.2609(7)	Cu(1)–P(6)	2.2957(12)
Cu(2)–P(5)	2.3193(6)	Cu(2)–P(2)	2.2872(12)
Cu(3) –P(2)	2.2540(6)	Cu(2)–P(3)	2.2803(11)
Cu(3)–P(3)	2.2838(6)	Cu(3) –P(4)	2.2787(10)
C(104)–C(117)	1.212(3)	Cu(3)–P(5)	2.2826(11)
C(113)–C(119)	1.211(3)	C(1)–C(2)	1.205(6)
C(18)–O(1)	1.213(4)	C(16)–C(17)	1.222(6)
C(92)–O(2)	1.232(3)	C(9)–O(1)	1.225(9)
C(104)–C(117)–Cu(1)	136.0(2)	C(24)–O(4)	1.250(6)
C(104)–C(117)–Cu(2)	127.07(19)	C(2)–C(1)–Cu(1)	130.3(3)
C(104)–C(117)–Cu(3)	137.85(19)	C(2)–C(1)–Cu(2)	151.4(4)
C(113)–C(119)–Cu(2)	138.5(2)	C(2)–C(1)–Cu(3)	124.2(3)
C(113)–C(119)–Cu(3)	146.1(2)	C(17)–C(16)–Cu(1)	147.9(4)
Cu(1)–C(117)–Cu(2)	81.45(8)	C(17)–C(16)–Cu(2)	128.6(3)
Cu(1)–C(117)–Cu(3)	80.48(8)	C(17)–C(16)–Cu(3)	130.8(3)
Cu(2)–C(117)–Cu(3)	67.65(7)	Cu(1)–C(1)–Cu(2)	73.36(13)
Cu(2)–C(119)–Cu(3)	74.57(10)	Cu(1)–C(1)–Cu(3)	70.35(13)
		Cu(2)–C(1)–Cu(3)	75.25(13)
		Cu(1)–C(16)–Cu(2)	73.20(13)
		Cu(1)–C(16)–Cu(3)	73.73(13)
		Cu(2)–C(16)–Cu(3)	73.47(13)

Table S6. Selected bond lengths (Å) and angles (°) for **4·BF$_4$** and **4·F**

4·BF$_4$		4·F	
Cu(1)···Cu(2)	2.6006(10)	Cu(1)···Cu(2)	2.6288(4)
Cu(1)···Cu(3)	2.6089(10)	Cu(1)···Cu(3)	2.6204(4)
Cu(2)···Cu(3)	2.5791(10)	Cu(2)···Cu(3)	2.6191(4)
C(1)–Cu(1)	2.182(5)	C(1)–Cu(1)	2.250(2)
C(1)–Cu(2)	2.217(5)	C(1)–Cu(2)	2.296(2)
C(1)–Cu(3)	2.344(5)	C(1)–Cu(3)	2.047(2)
C(17)–Cu(1)	2.220(5)	C(17)–Cu(1)	2.209(2)
C(17)–Cu(2)	2.203(5)	C(17)–Cu(2)	2.047(2)
C(17)–Cu(3)	2.111(5)	C(17)–Cu(3)	2.278(2)
Cu(1)–P(1)	2.2929(15)	Cu(1)–P(1)	2.2700(5)
Cu(1)–P(6)	2.2969(16)	Cu(1)–P(3)	2.2705(6)
Cu(2)–P(2)	2.2649(14)	Cu(2)–P(4)	2.2902(5)
Cu(2)–P(3)	2.2839(14)	Cu(2)–P(6)	2.2849(6)
Cu(3) –P(4)	2.2874(14)	Cu(3)–P(2)	2.2904(5)
Cu(3)–P(5)	2.2633(14)	Cu(3)–P(5)	2.2793(6)
C(1)–C(2)	1.134(8)	C(1)–C(2)	1.211(3)
C(17)–C(18)	1.185(8)	C(17)–C(18)	1.215(3)
C(9)–O(1)	1.223(11)	C(9)–O(1)	1.240(3)
C(25)–O(3)	1.202(8)	C(25)–O(3)	1.224(3)
C(2)–C(1)–Cu(1)	145.1(5)	C(2)–C(1)–Cu(1)	119.21(17)
C(2)–C(1)–Cu(2)	132.2(5)	C(2)–C(1)–Cu(2)	122.50(16)
C(2)–C(1)–Cu(3)	136.2(5)	C(2)–C(1)–Cu(3)	160.15(18)
C(18)–C(17)–Cu(1)	140.5(5)	C(18)–C(17)–Cu(1)	119.95(17)
C(18)–C(17)–Cu(2)	134.2(4)	C(18)–C(17)–Cu(2)	156.79(17)
C(18)–C(17)–Cu(3)	134.6(5)	C(18)–C(17)–Cu(3)	124.96(16)
Cu(1)–C(1)–Cu(2)	72.48(17)	Cu(1)–C(1)–Cu(2)	70.66(6)
Cu(1)–C(1)–Cu(3)	70.30(16)	Cu(1)–C(1)–Cu(3)	74.98(7)
Cu(2)–C(1)–Cu(3)	68.82(16)	Cu(2)–C(1)–Cu(3)	73.93(6)
Cu(1)–C(17)–Cu(2)	72.02(16)	Cu(1)–C(17)–Cu(2)	76.18(7)
Cu(1)–C(17)–Cu(3)	74.03(17)	Cu(1)–C(17)–Cu(3)	71.43(6)
Cu(2)–C(17)–Cu(3)	73.40(17)	Cu(2)–C(17)–Cu(3)	74.32(7)

Table S7. Photophysical data of ligands **L1**−**L4** at 298 K.

ligands	medium	λ_{abs} / nm (ε / dm^{3}mol^{-1}cm^{-1})	λ_{em} / nm
L1	DMSO	268 (26790), 312 (11870)	469
	solid		No-emission
L2	DMSO	290 (19670)	468
	solid		438, 469
L3	DMSO	288 (28480)	468
	solid		424, 463
L4	DMSO	292 (28860)	468
	solid		439, 469
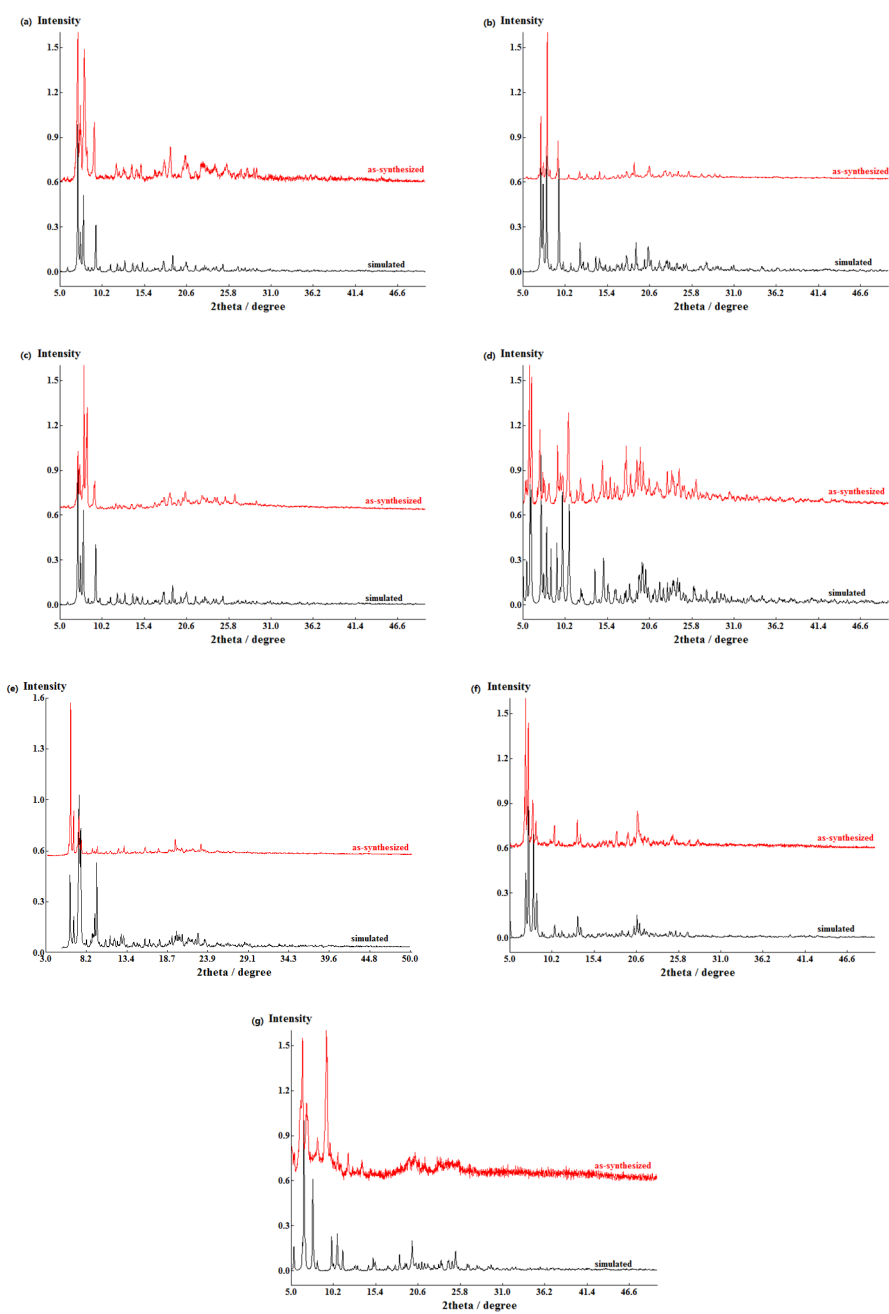
Figure S1. Powder X-ray diffraction patterns for the anion complexes: as-synthesized (red) and simulated from the single-crystal diffraction data (black), (a) **1·BF₄**; (b) **1·PF₆**; (c) **1·ClO₄**; (d) **2·BF₄**; (e) **3·BF₄**; (f) **4·BF₄**; and (g) **4·F**.
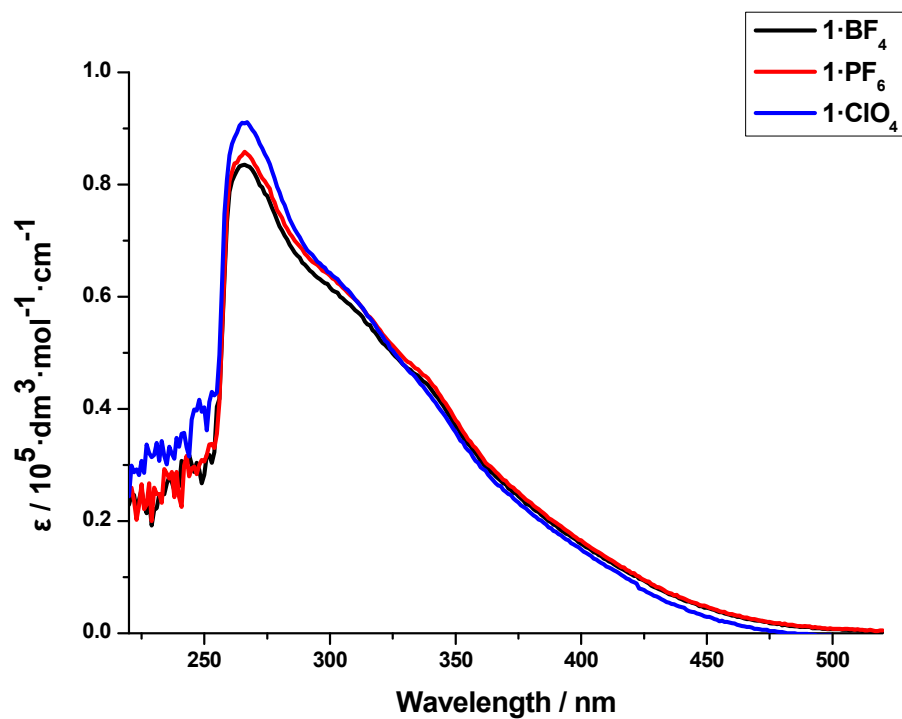
Figure S2. Electronic absorption spectra of **1·BF₄**, **1·PF₆**, and **1·ClO₄** in DMSO at 298 K.
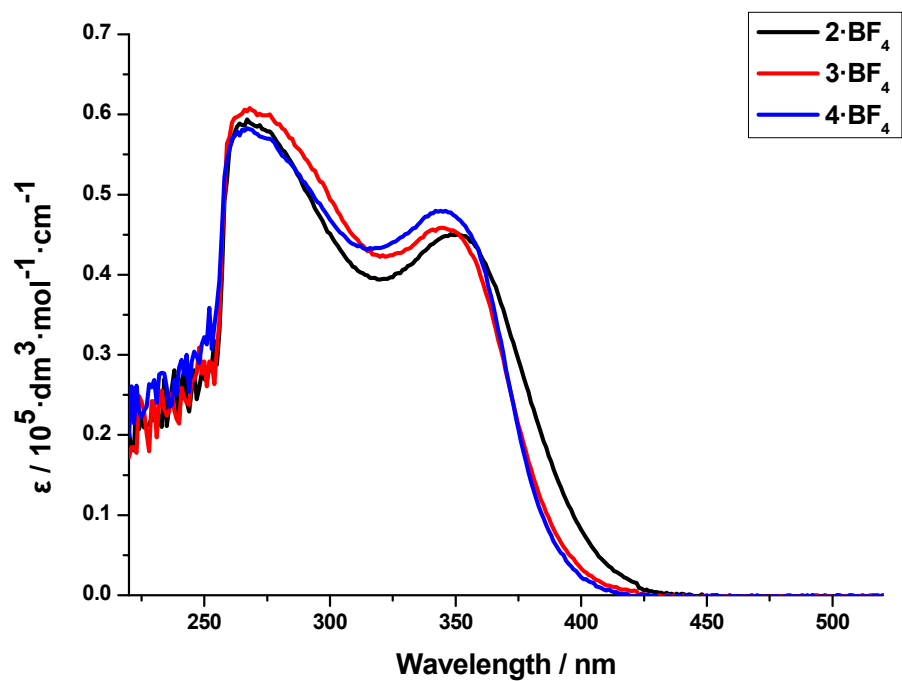
Figure S3. Electronic absorption spectra of **2·BF₄**–**4·BF₄** in DMSO at 298 K.
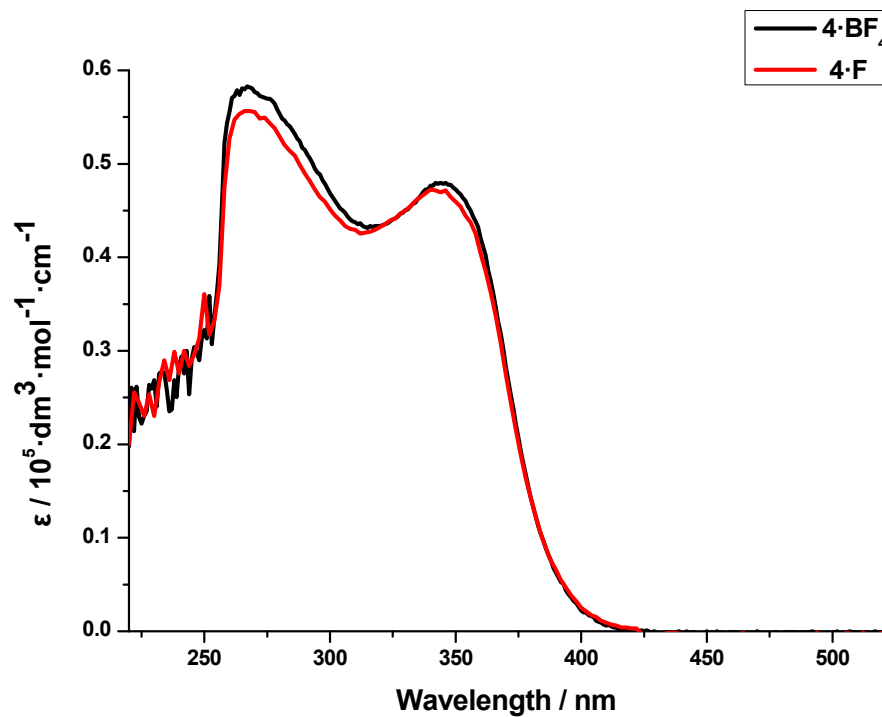
Figure S4. Electronic absorption spectra of **4·BF₄**, and **4·F** in DMSO at 298 K.
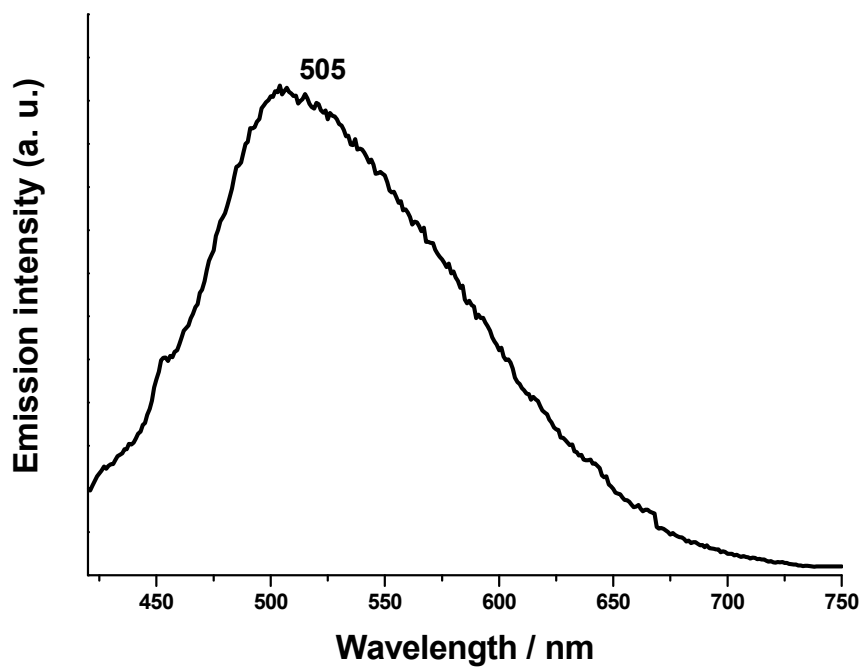
Figure S5. Emission spectrum of **1·BF₄** in the solid state at 298 K (λ_{ex} = 371 nm).
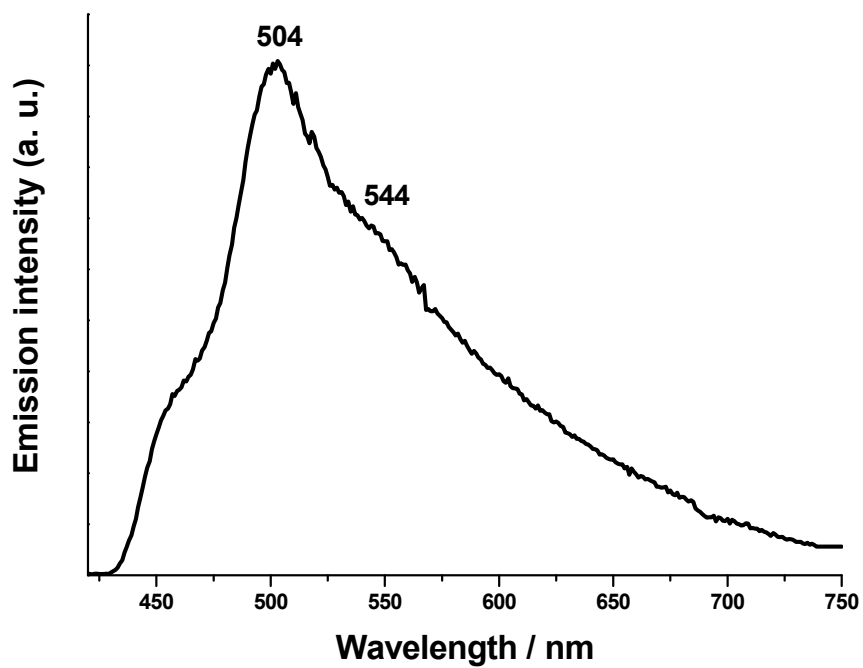
Figure S6. Emission spectrum of **1·PF₆** in the solid state at 298 K (λ_{ex} = 372 nm).
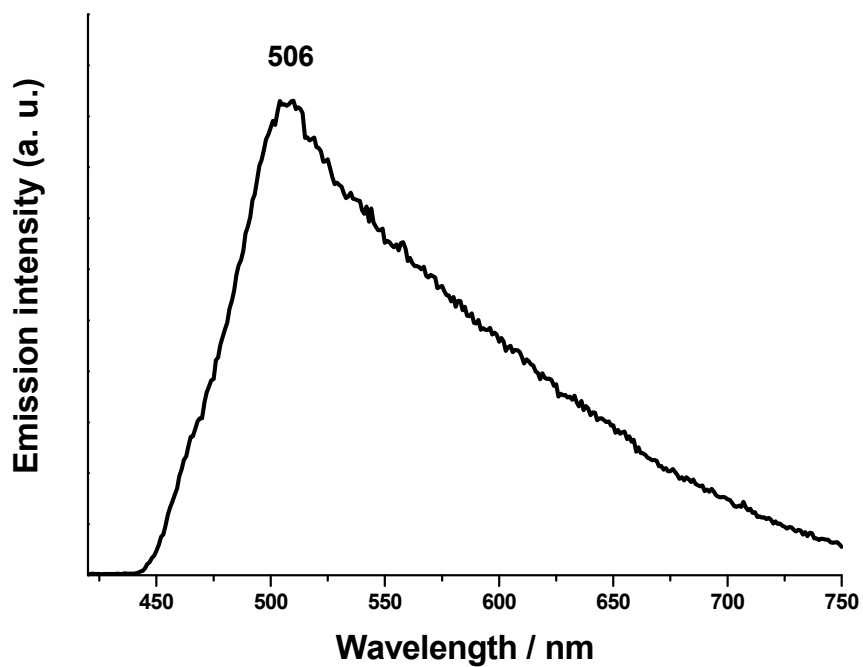
Figure S7. Emission spectrum of **1·ClO₄** in the solid state at 298 K (λ_{ex} = 371 nm).
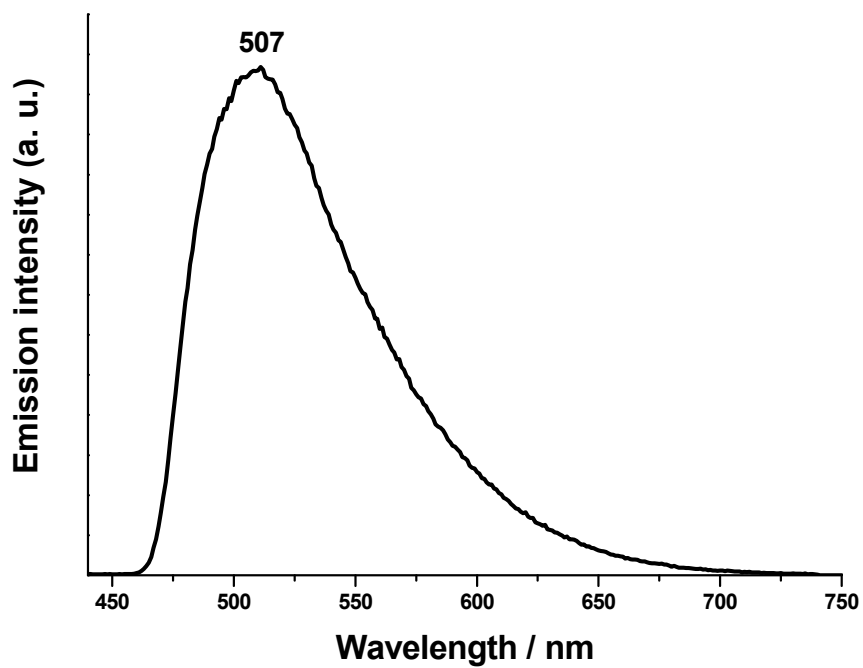
Figure S8. Emission spectrum of **2·BF₄** in the solid state at 298 K (λ_{ex} = 428 nm).
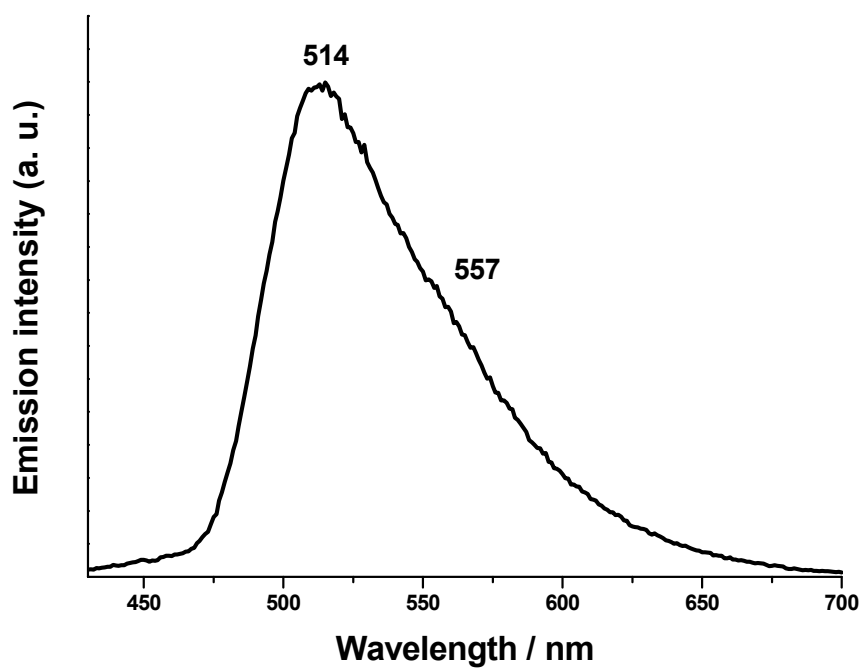
Figure S9. Emission spectrum of **4·BF₄** in the solid state at 298 K (λ_{ex} = 407 nm).
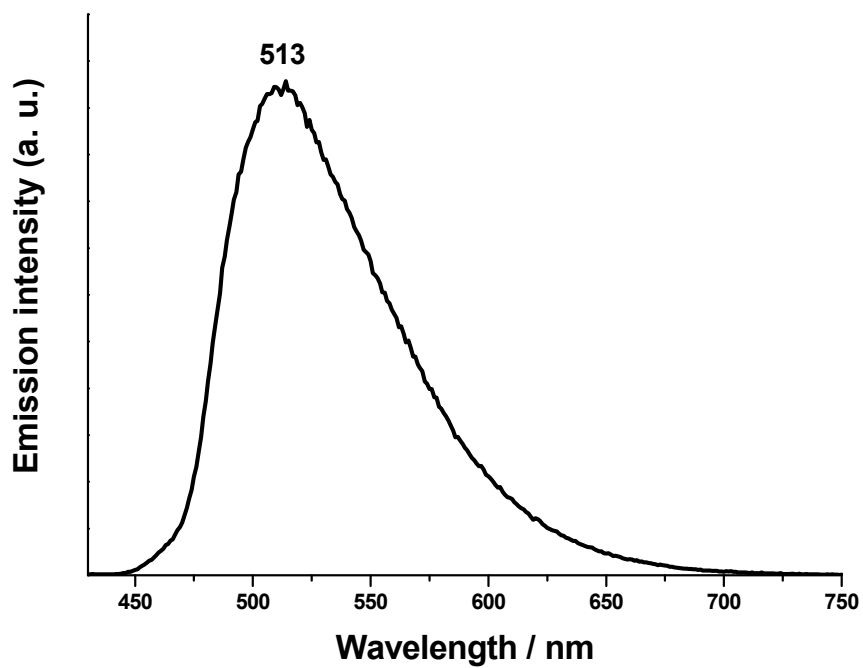
Figure S10. Emission spectrum of **4·F** in the solid state at 298 K (λ_{ex} = 408 nm).
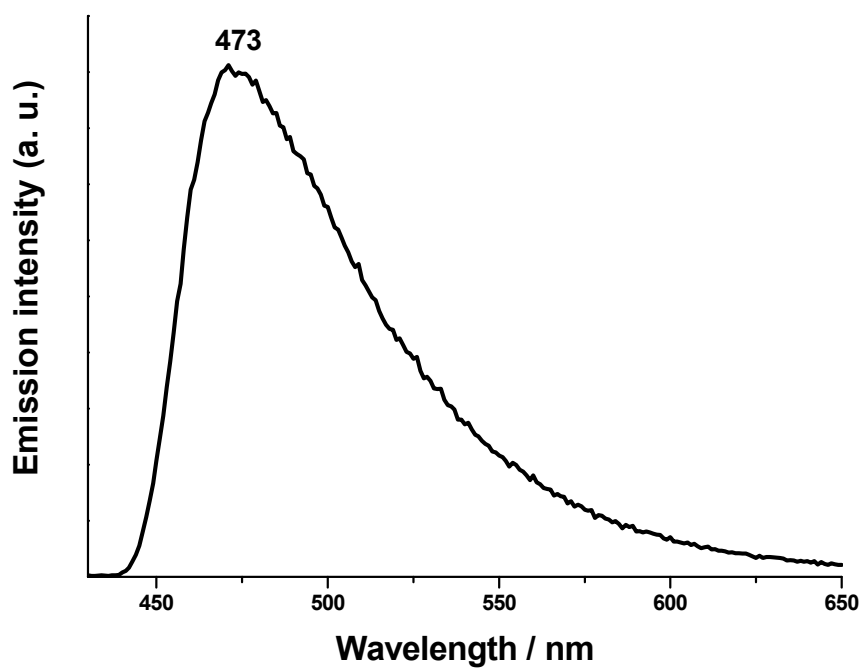
Figure S11. Emission spectrum of **1·BF₄** (3.96×10^{-5} mol dm^{-3}) in DMSO at 298 K (λ_{ex} = 380 nm).
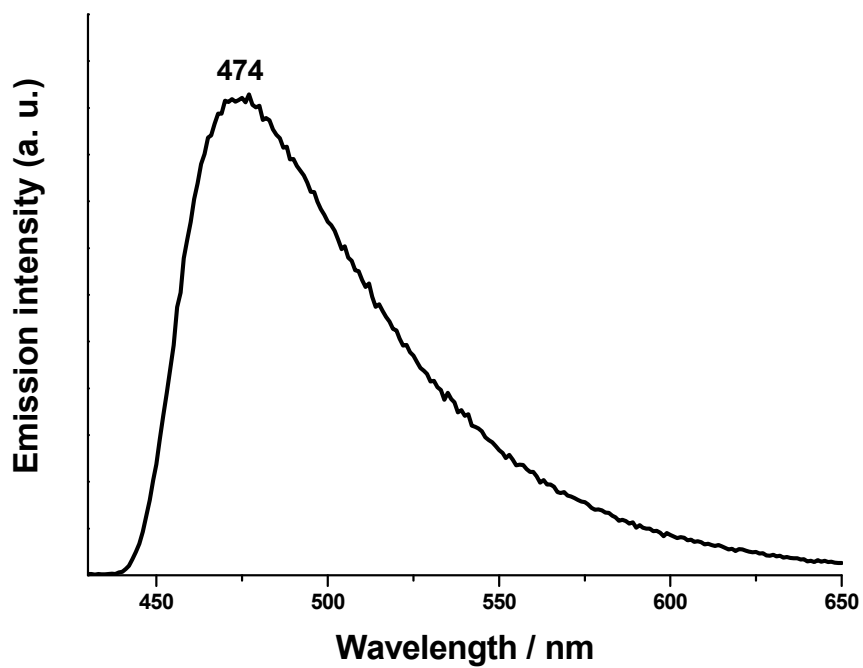
Figure S12. Emission spectrum of **1·PF₆** (3.96×10⁻⁵ mol dm⁻³) in DMSO at 298 K (λ_{ex} = 380 nm).
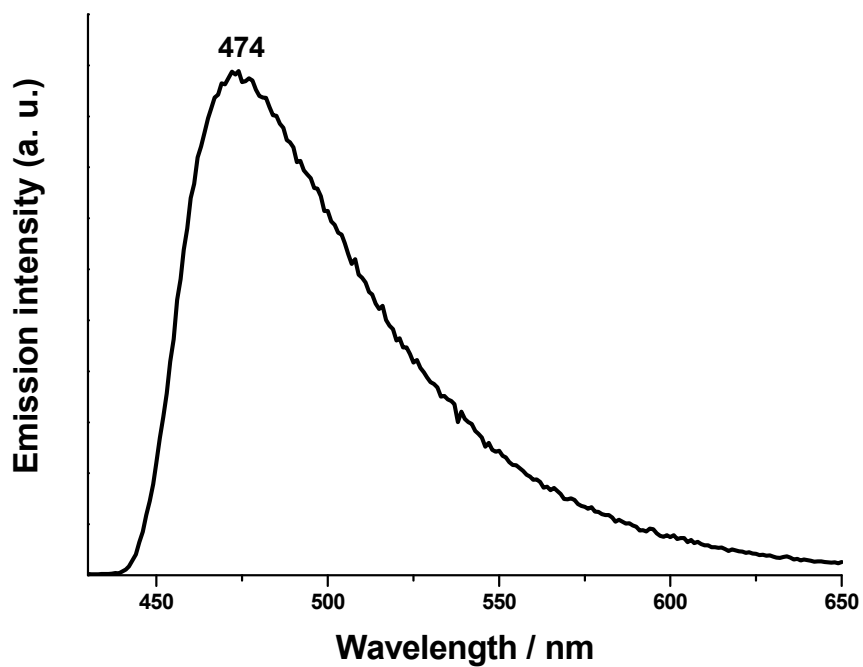
Figure S13. Emission spectrum of **1·ClO₄** (3.96×10⁻⁵ mol dm⁻³) in DMSO at 298 K (λ_{ex} = 380 nm).
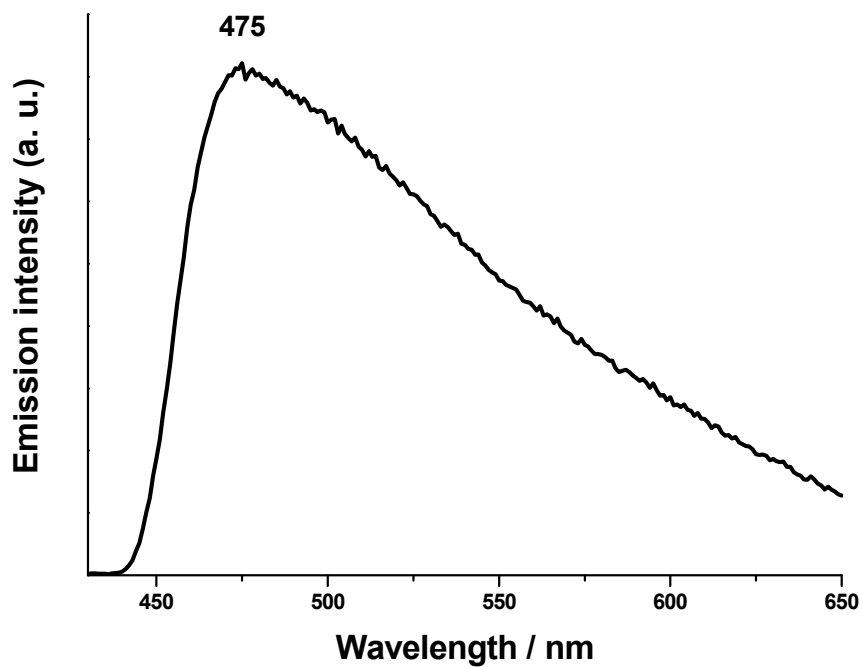
Figure S14. Emission spectrum of **2·BF₄** (3.96×10⁻⁵ mol dm⁻³) in DMSO at 298 K (λₑₓ = 380 nm).
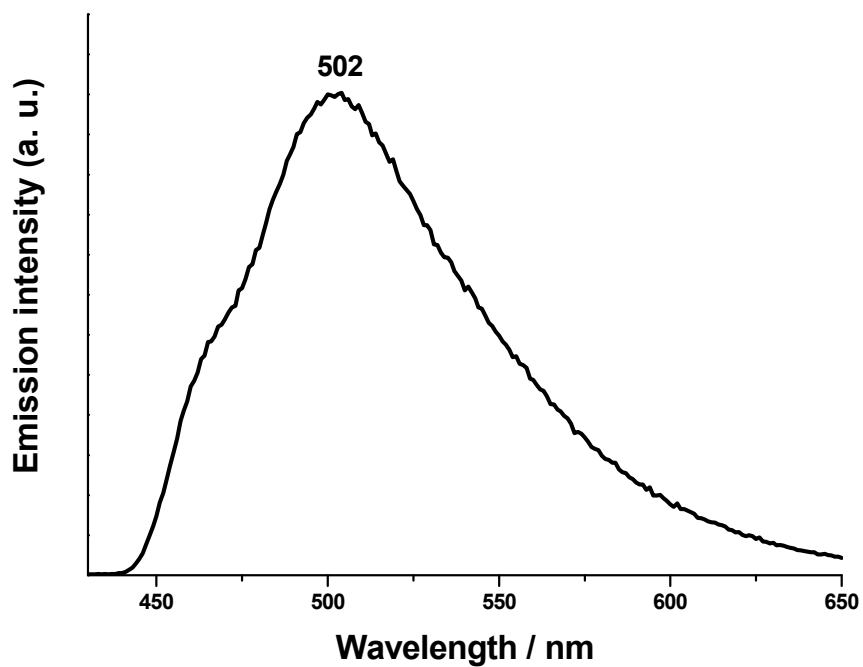
Figure S15. Emission spectrum of **3·BF₄** (3.96×10⁻⁵ mol dm⁻³) in DMSO at 298 K (λₑₓ = 380 nm).
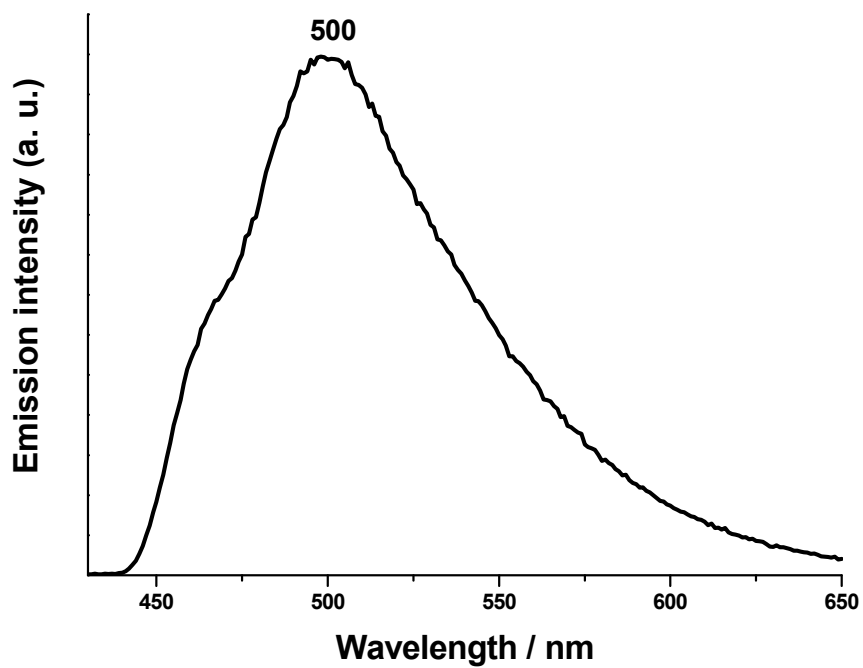
Figure S16. Emission spectrum of **4·BF₄** (3.96×10^{-5} mol dm^{-3}) in DMSO at 298 K (λ_{ex} = 380 nm).
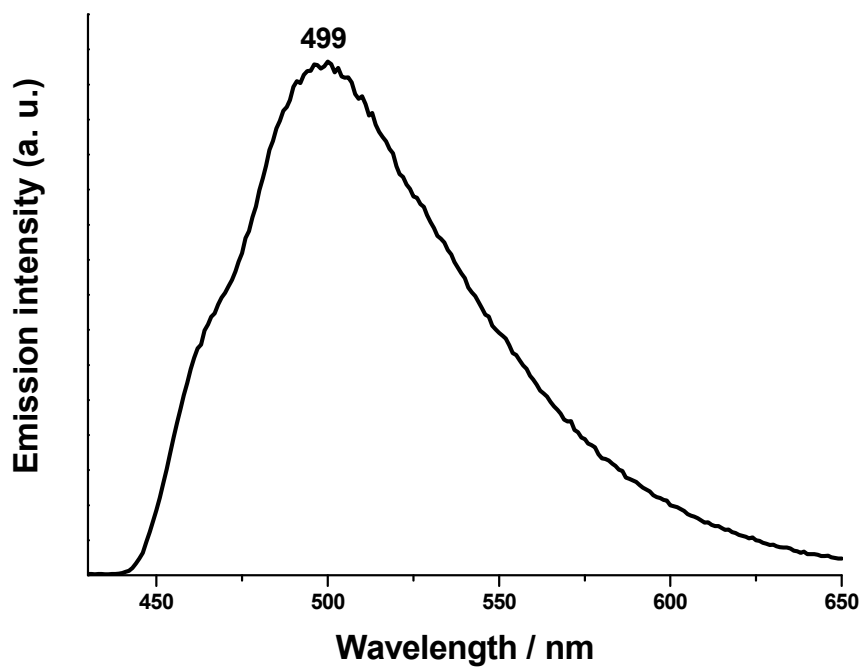
Figure S17. Emission spectrum of **4·F** (3.96×10^{-5} mol dm^{-3}) in DMSO at 298 K (λ_{ex} = 380 nm).
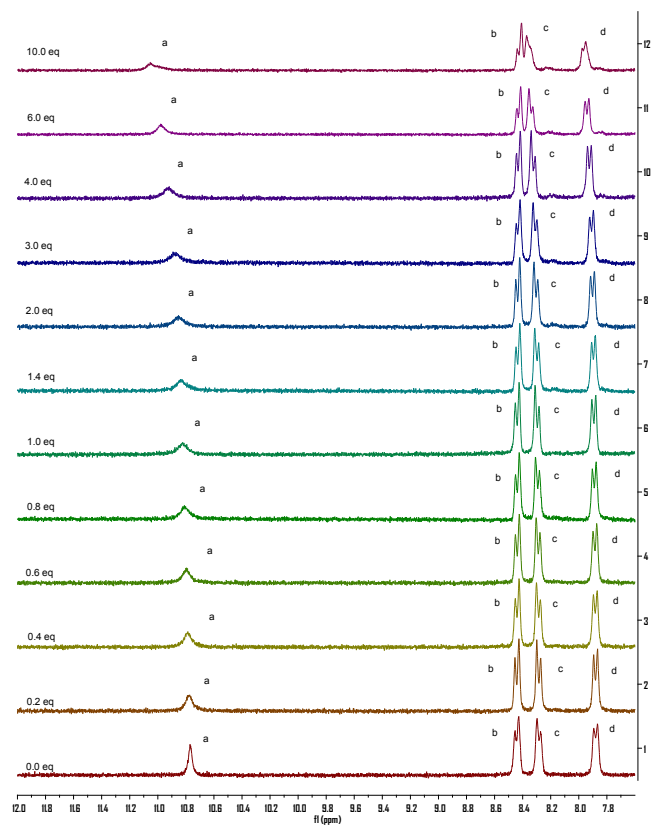
Figure S18. The ^{1}H NMR spectral changes of **1·BF$_4$** upon addition of Cl$^-$ in DMSO-d$_6$ at 298 K.
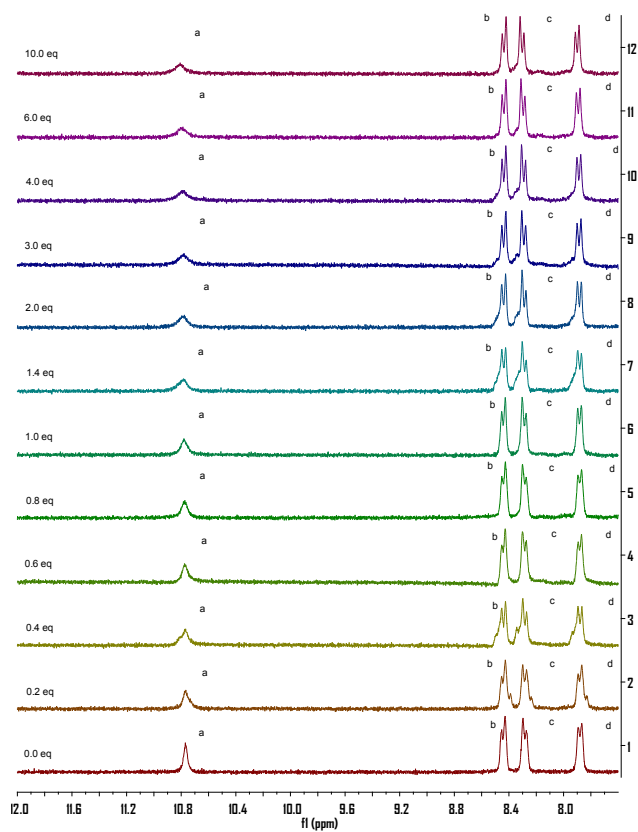
Figure S19. The ^{1}H NMR spectral changes of **1·BF$_4$** upon addition of Br$^-$ in DMSO-d$_6$ at 298 K.
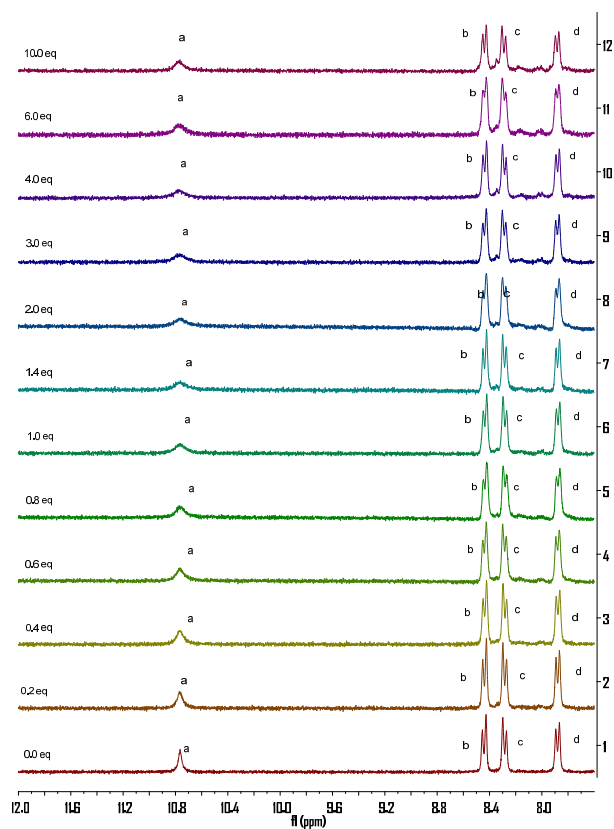
Figure S20. The ^{1}H NMR spectral changes of **1·BF₄** upon addition of I⁻ in DMSO-d₆ at 298 K.
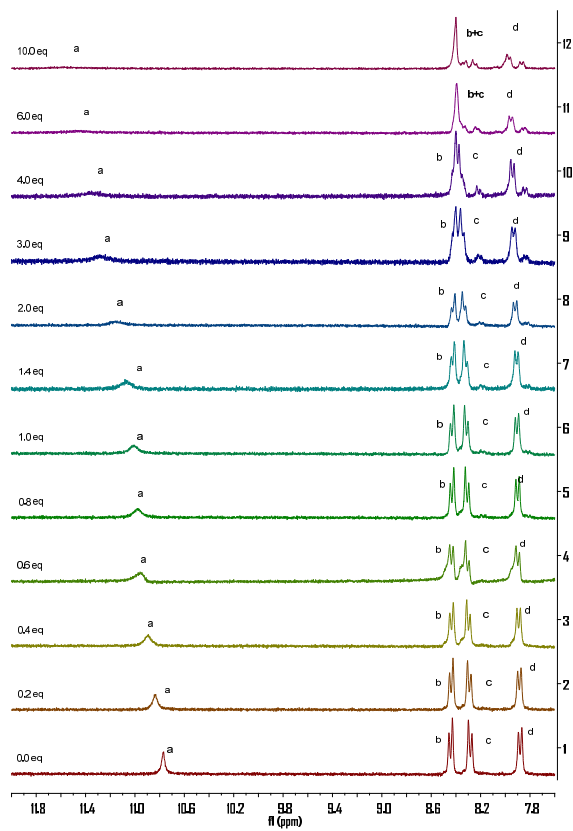
Figure S21. The ^{1}H NMR spectral changes of **1·BF₄** upon addition of OAc⁻ in DMSO-d₆ at 298 K.
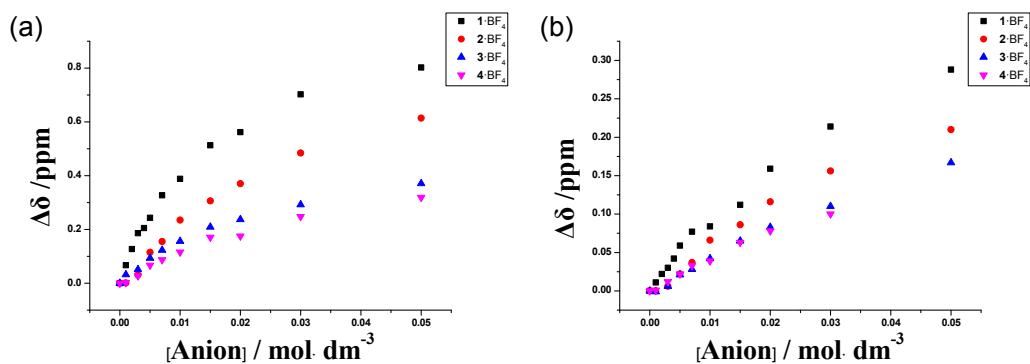
Figure S22. The shifts of the signals of amide N–H (H$_a$) of **1·BF$_4$**–**4·BF$_4$** upon addition of the same anion ((a) OAc$^-$; (b) Cl$^-$) with different concentrations in DMSO–d_6 at 298 K.
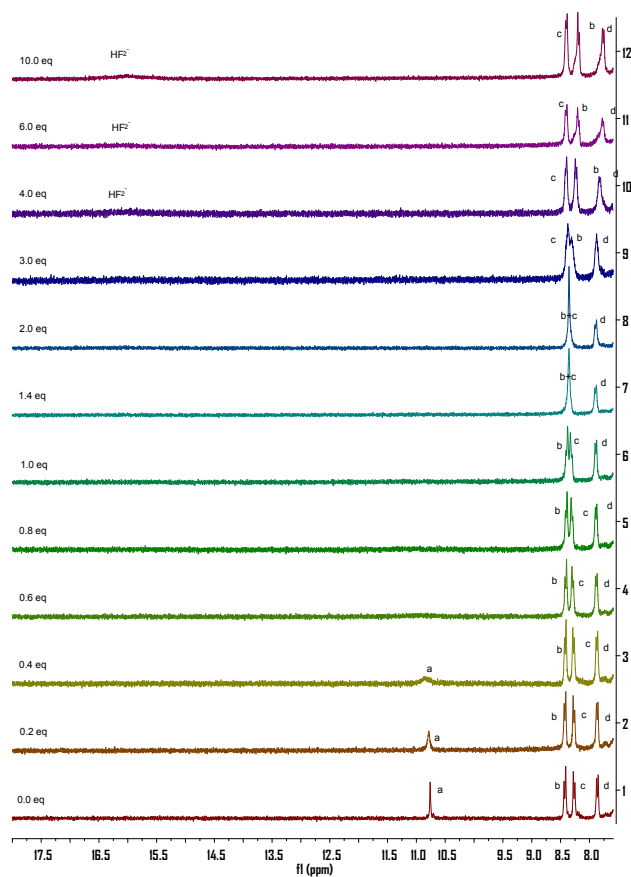
Figure S23. The ^{1}H NMR spectral changes of **1·BF$_4$** upon addition of F$^-$ in DMSO-d$_6$ at 298 K.
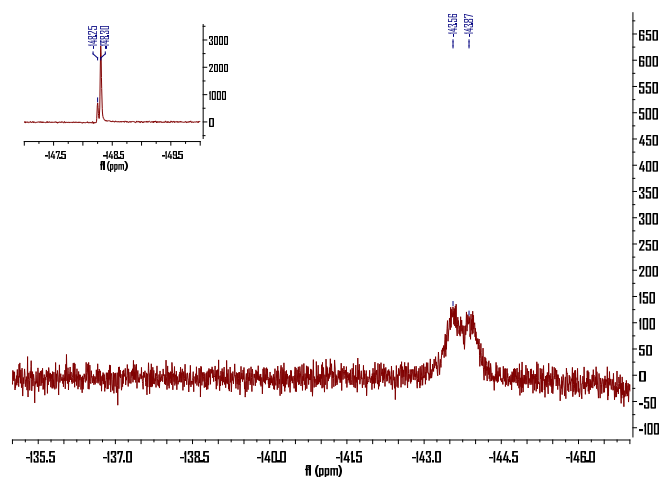
Figure S24. The ^{19}F NMR (DMSO-d$_6$, 298 K) spectrum of **1·BF$_4$** (5.0×10^{-3} mol dm^{-3}) + 10 eq of F$^-$. Insert: the ^{19}F NMR (DMSO-d$_6$, 298 K) spectrum of BF$_4^-$ in this system.
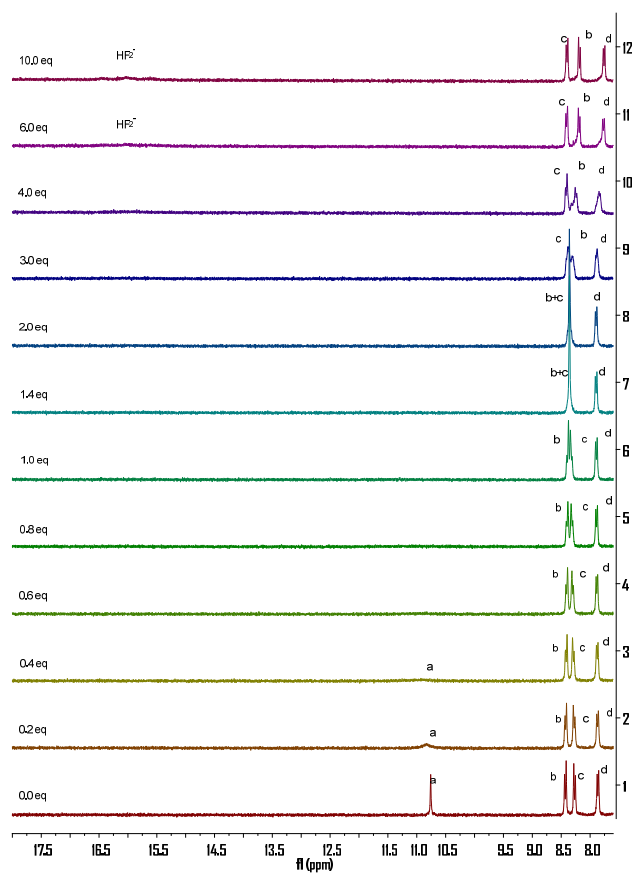
Figure S25. The ^1H NMR spectral changes of **1·PF$_6$** upon addition of F$^-$ in DMSO-d$_6$ at 298 K.
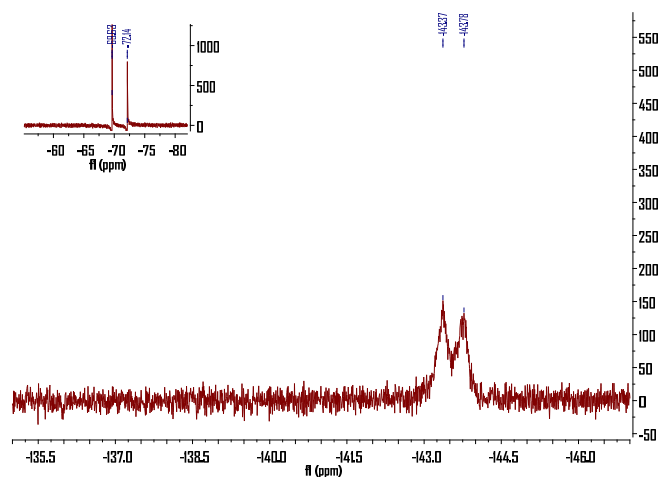
Figure S26. The ^{19}F NMR (DMSO-d$_6$, 298 K) spectrum of **1·PF$_6$** (5.0×10^{-3} mol dm^{-3}) + 10 eq of F$^-$. Insert: the ^{19}F NMR (DMSO-d$_6$, 298 K) spectrum of PF$_6^-$ in this system.
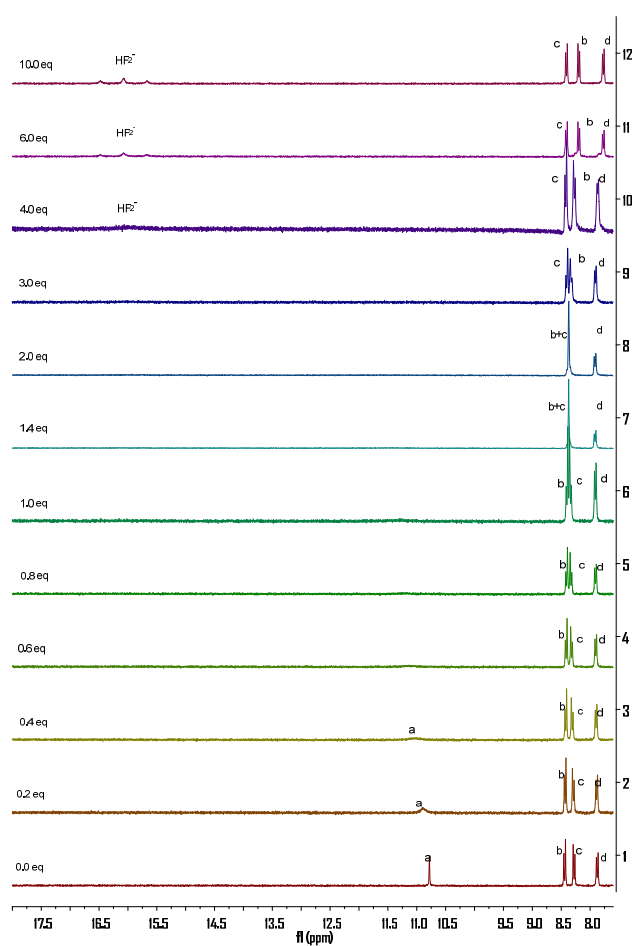
Figure S27. The ^{1}H NMR spectral changes of **1·ClO$_4$** upon addition of F$^-$ in DMSO-d$_6$ at 298 K.
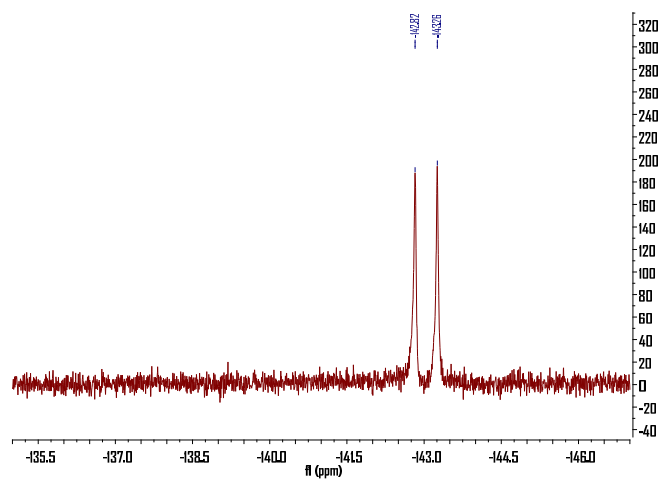
Figure S28. The ^{19}F NMR (DMSO-d$_6$, 298 K) spectrum of **1·ClO$_4$** (5.0×10^{-3} mol dm^{-3}) + 10 eq of F$^-$.
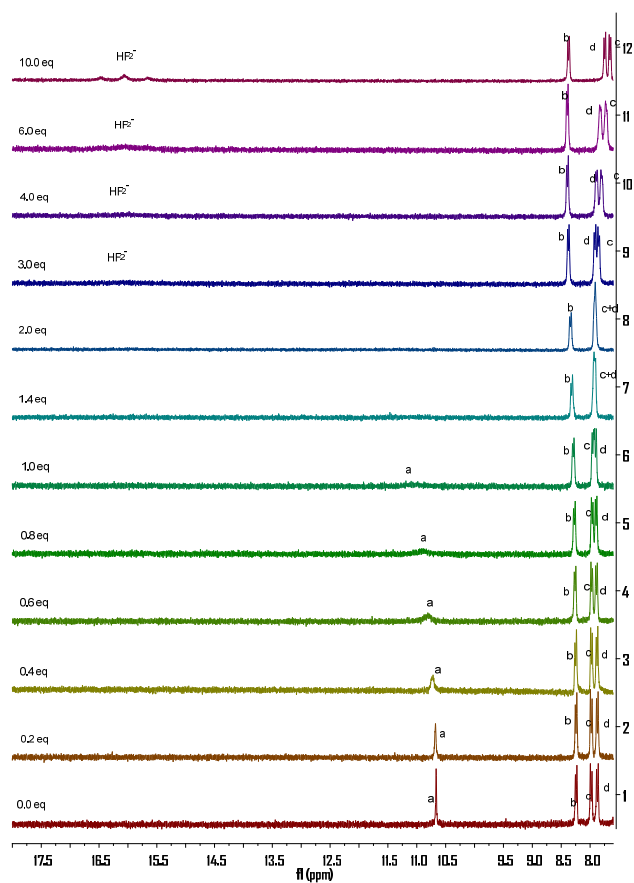
Figure S29. The ^1H NMR spectral changes of **2·BF$_4$** upon addition of F$^-$ in DMSO-d$_6$ at 298 K.
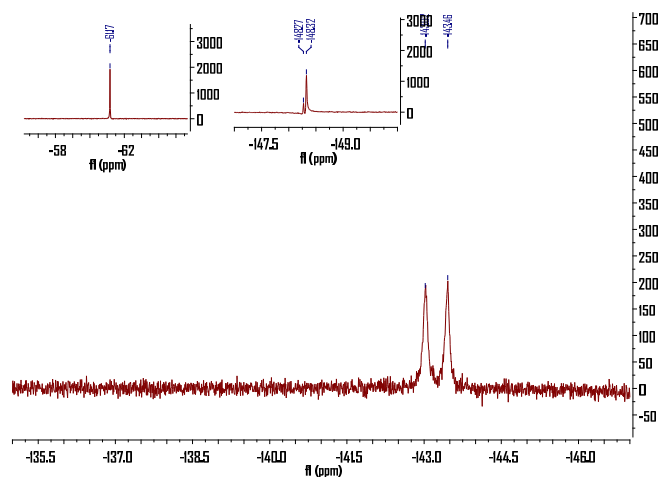
Figure S30. The ^{19}F NMR (DMSO-d$_6$, 298 K) spectrum of **2·BF$_4$** (5.0×10^{-3} mol dm^{-3}) + 10 eq of F$^-$. Insert: the ^{19}F NMR (DMSO-d$_6$, 298 K) spectrum of CF$_3$ group (left) and BF$_4^-$ (right) in this system.
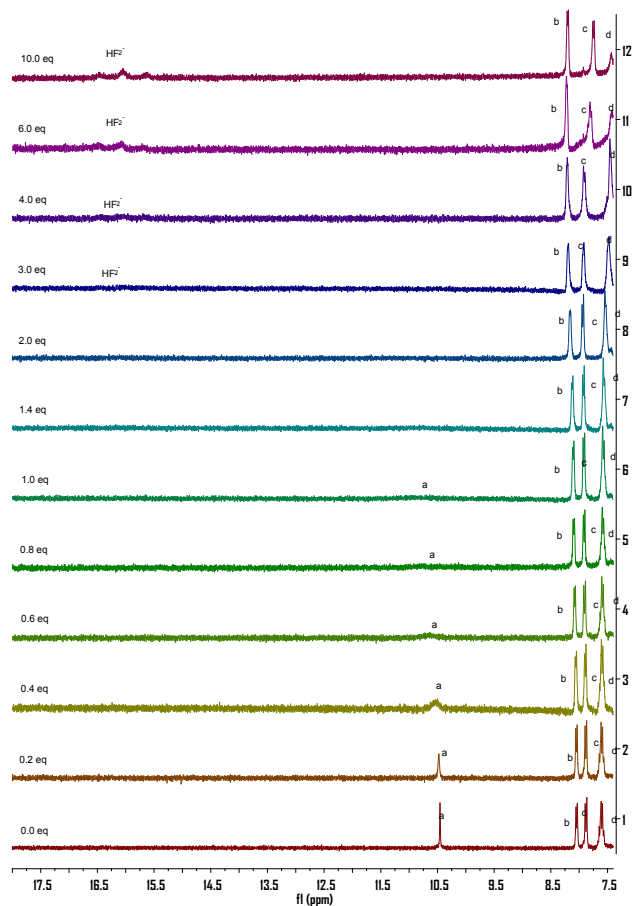
Figure S31. The ^{1}H NMR spectral changes of **3·BF$_4$** upon addition of F$^-$ in DMSO-d$_6$ at 298 K.
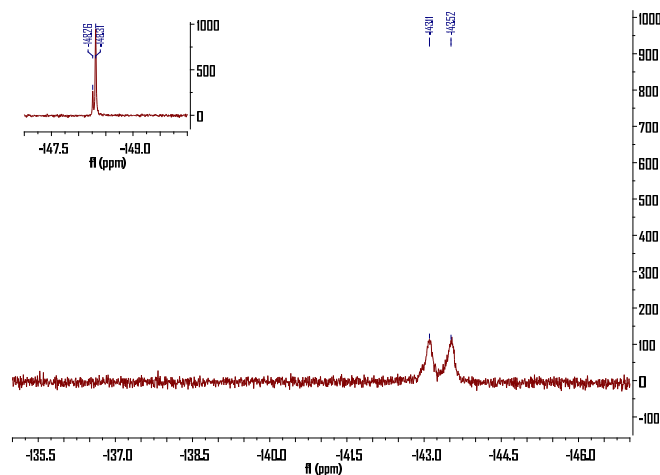
Figure S32. The ^{19}F NMR (DMSO-d$_6$, 298 K) spectrum of **3·BF$_4$** (5.0×10^{-3} mol dm^{-3}) + 10 eq of F$^-$. Insert: the ^{19}F NMR (DMSO-d$_6$, 298 K) spectrum of BF$_4^-$ in this system.
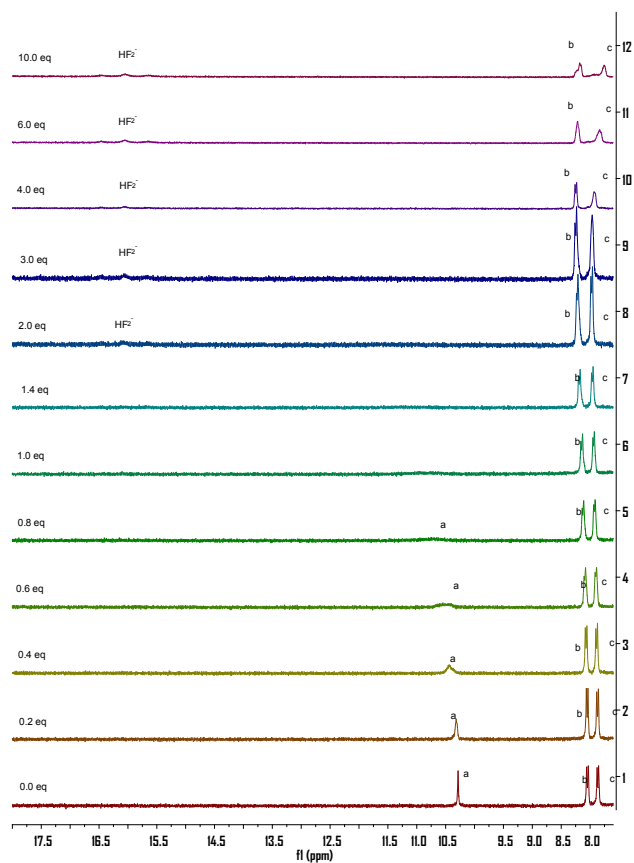
Figure S33. The ^{1}H NMR spectral changes of **4·BF$_4$** upon addition of F$^-$ in DMSO-d$_6$ at 298 K.
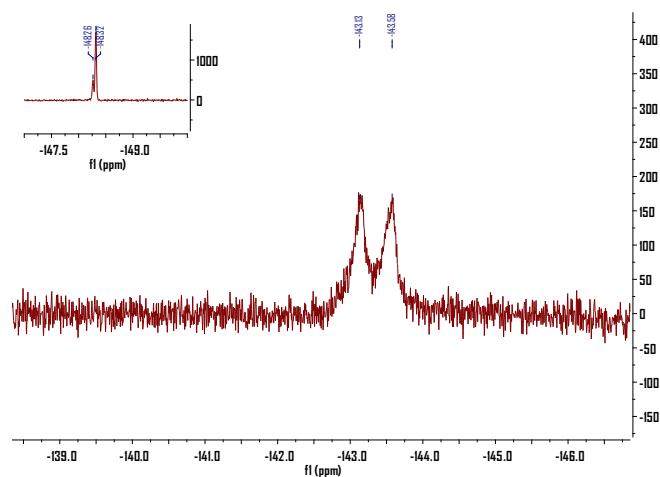
Figure S34. The ^{19}F NMR (DMSO-d$_6$, 298 K) spectrum of **4·BF$_4$** (5.0×10^{-3} mol dm^{-3}) + 10 eq of F$^-$. Insert: the ^{19}F NMR (DMSO-d$_6$, 298 K) spectrum of BF$_4^-$ in this system.

1·BF$_4$ **1·BF$_4$**+F$^-$ **1·BF$_4$**+Cl$^-$ **1·BF$_4$**+Br$^-$ **1·BF$_4$**+I$^-$ **1·BF$_4$**+OAc$^-$

Figure S35. Colors of **1·BF$_4$** (1.98×10^{-5} mol dm^{-3}) in DMSO in the presence of 100 eq F$^-$, Cl$^-$, Br$^-$，I$^-$ and OAc$^-$.
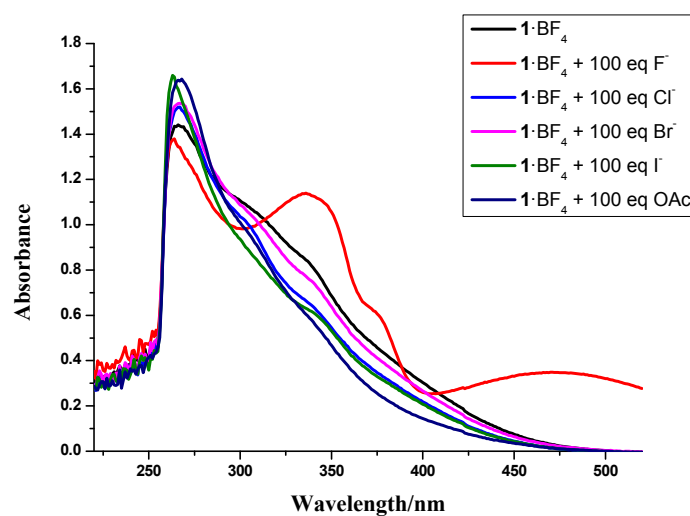
Figure S36. The UV−vis spectra of **1·BF$_4$** (1.98×10^{-5} mol dm^{-3}) in DMSO in the presence of 100 eq F$^-$, Cl$^-$, Br$^-$, I$^-$ and OAc$^-$.
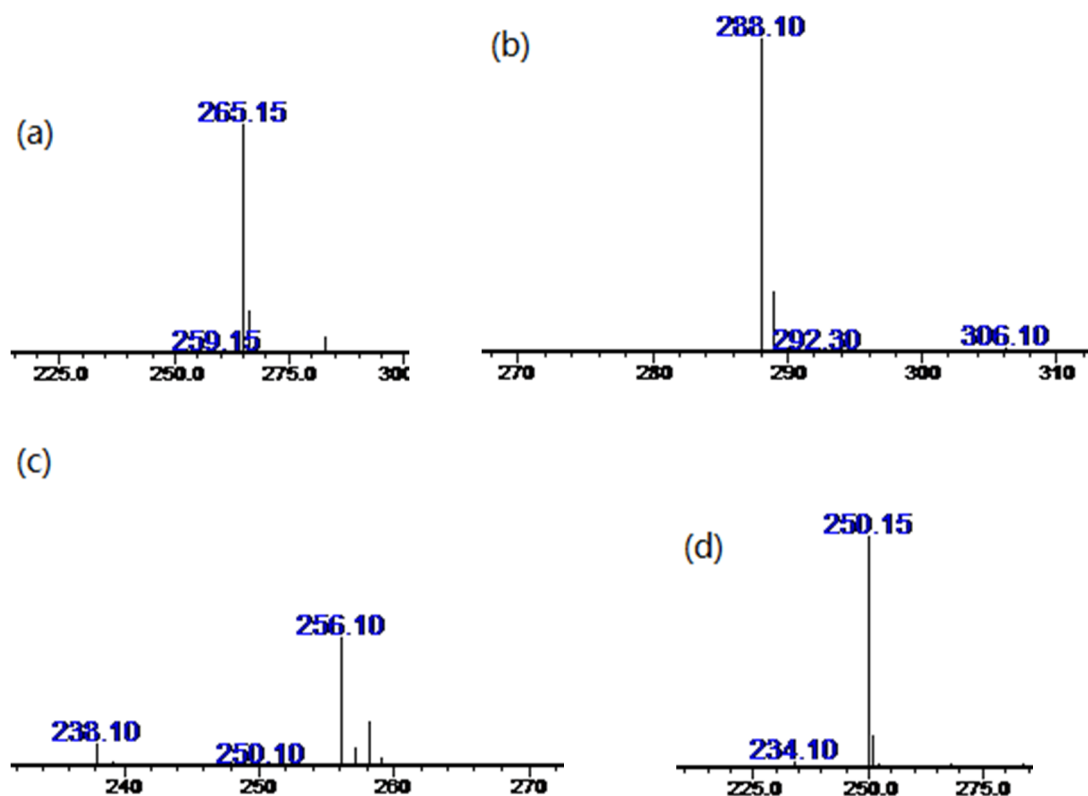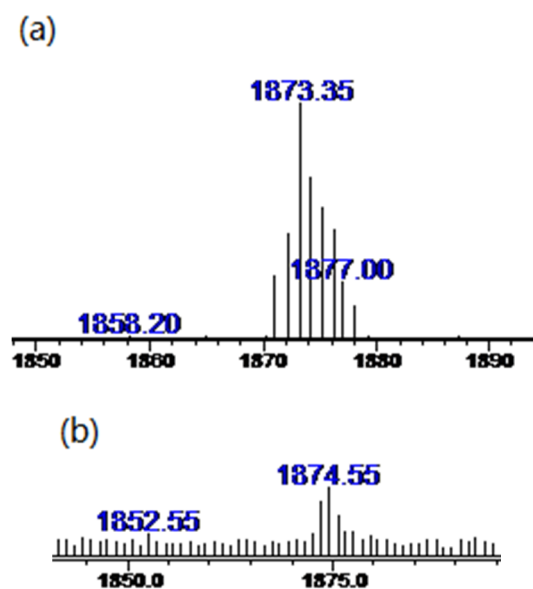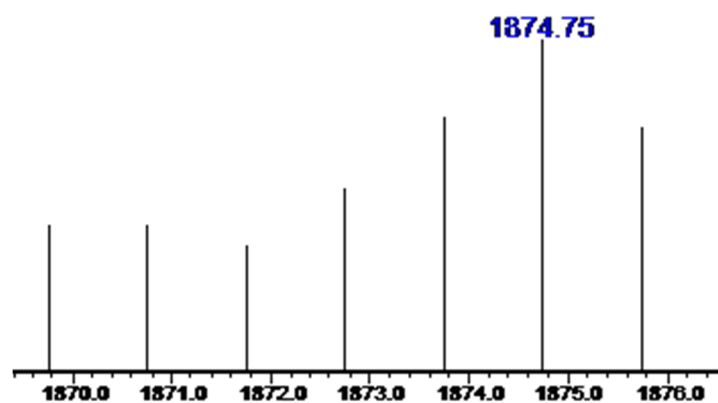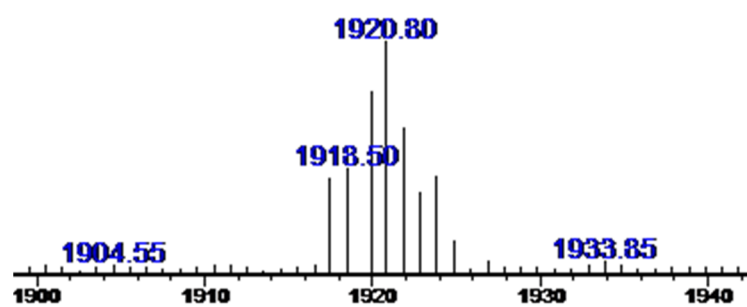
Figure S37. The ESI-MS spectra of ligands, (a) **L1**; (b) **L2**; (c) **L3**; (d) **L4**. (partial spectra are shown due to the large scale of the spectra)
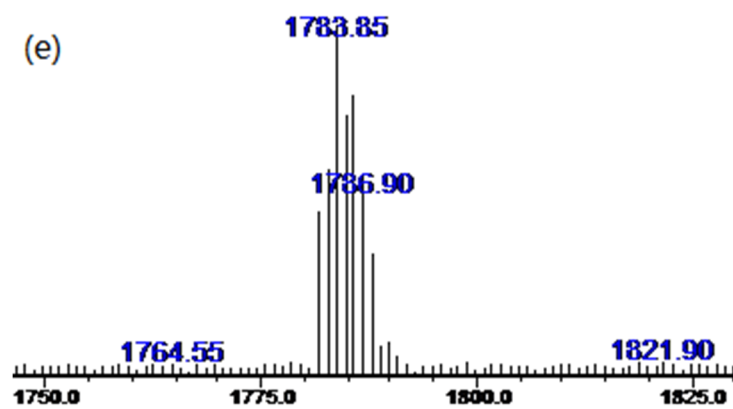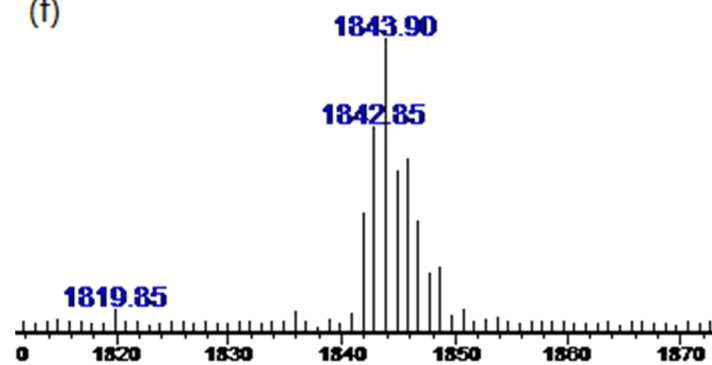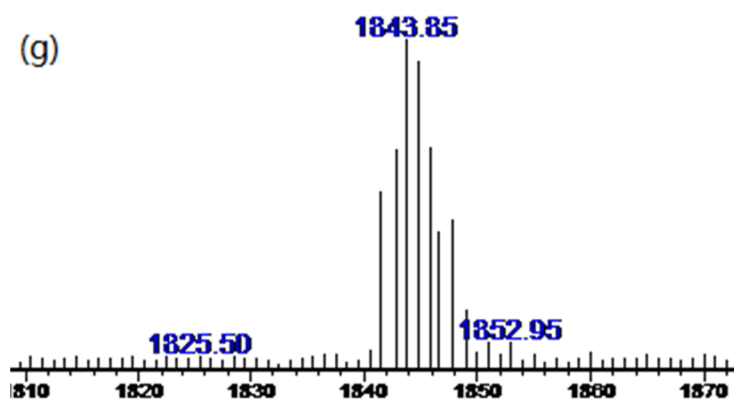
(c)

(d)

(e)

(f)

Figure S38. The ESI-MS spectra of complexes, (a) **1·BF₄**; (b) **1·PF₆**; (c) **1·ClO₄**; (d) **2·BF₄**; (e) **3·BF₄**; (f) **4·BF₄**; and (g) **4·F**. (partial spectra are shown due to the large scale of the spectra)